Electronic Supplementary Information (ESI) for

Tetraphenylethylene-based microporous organic polymers: insight into structure geometry, porosity, and CO_2/CH_4 selectivity

Hui Li,[†,‡] Xuesong Ding,*[,†] and Bao-Hang Han*[,†]

[†] *CAS Key Laboratory of Nanosystem and Hierarchical Fabrication, CAS Center for Excellence in Nanoscience, National Center for Nanoscience and Technology, Beijing 100190, China;*

[‡] *University of Chinese Academy of Sciences, Beijing 100049, China*

Tel: +86 10 8254 5576; Email: hanbh@nanoctr.cn

Tel: +86 10 8254 5708; Email: dingxs@nanoctr.cn

Contents

Section A. Figure of ketal-linked structure

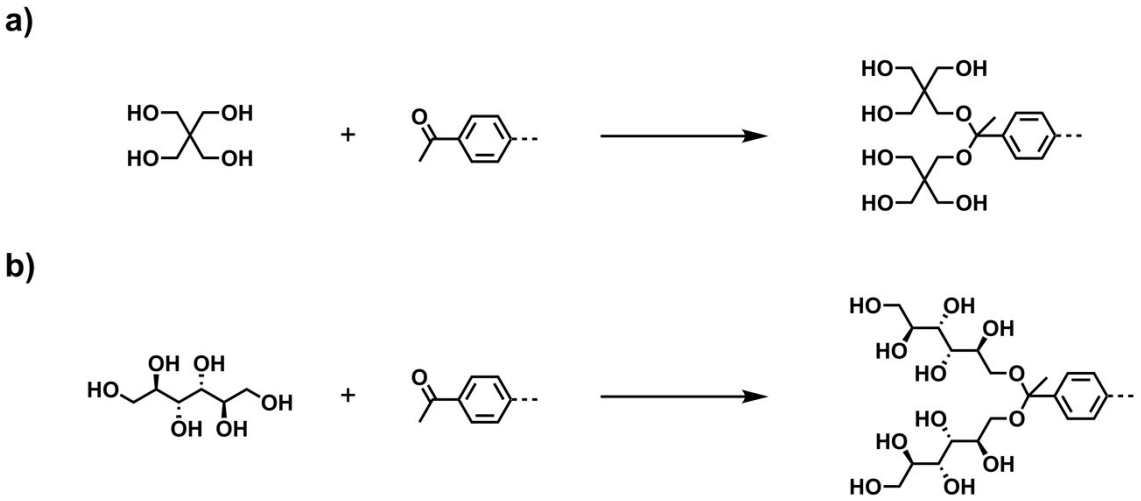

Fig. S1 Branched ketal-linked structures in (a) **PTPOPs** and (b) **MTPOPs**.

Section B. TGA curves

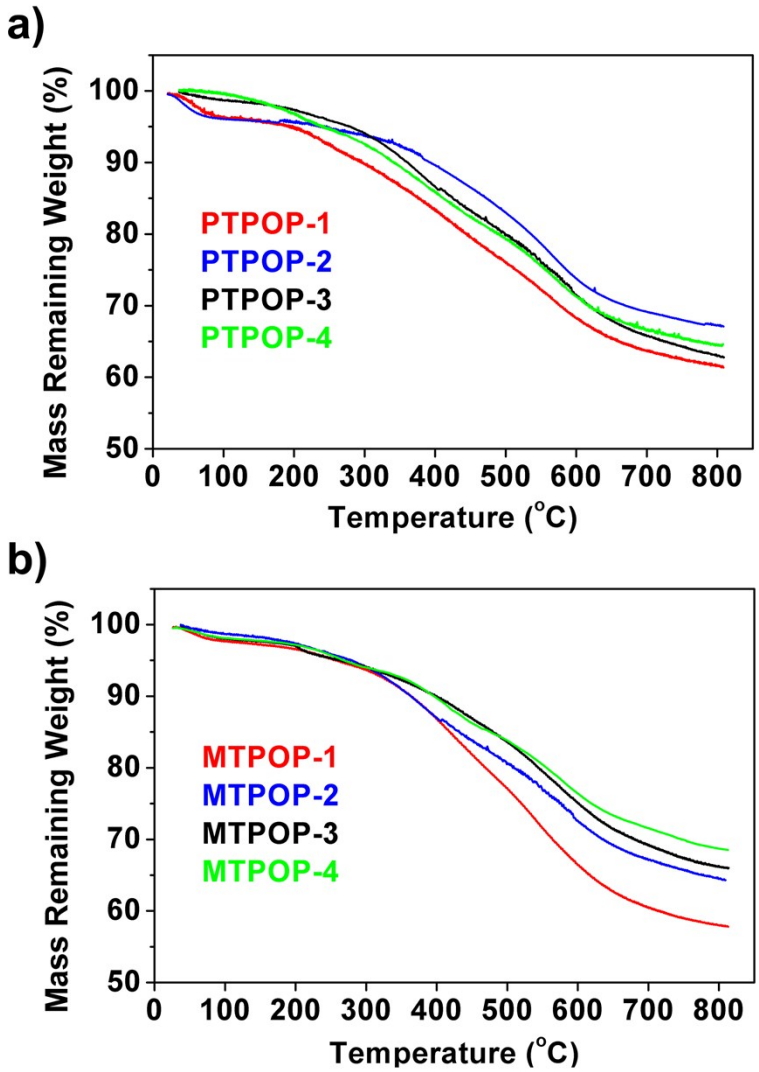

Fig. S2 TGA curves of **PTPOP-1–4** and **MTPOP-1–4**.

Section C. FE-SEM images

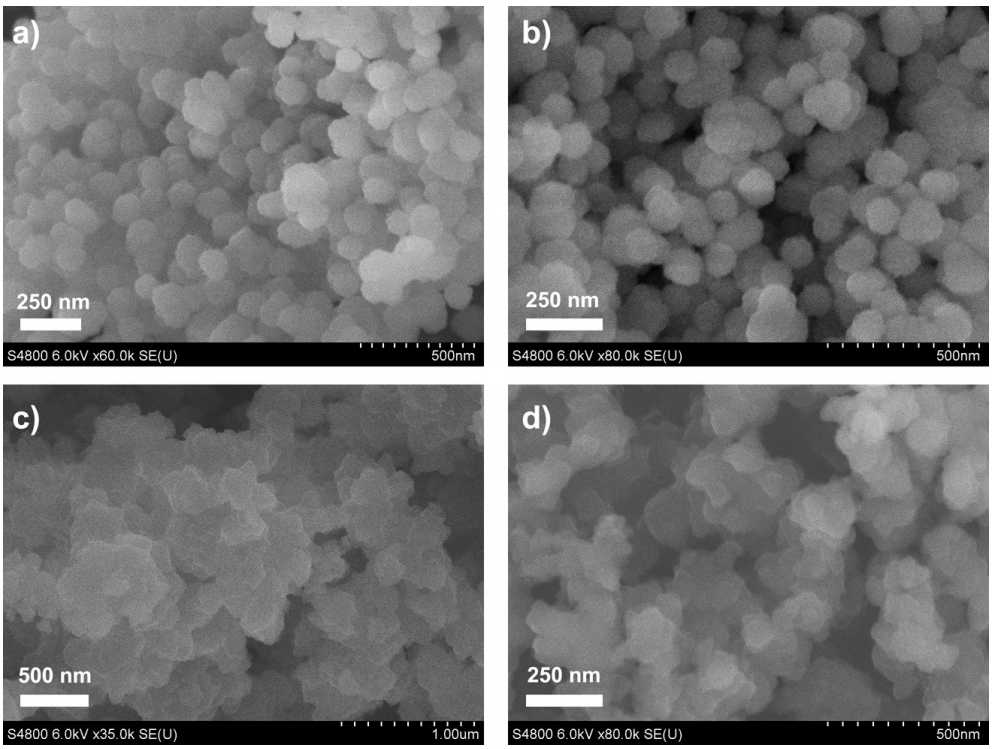

Fig. S3 FE-SEM images of **PTPOP-1** (a), **PTPOP-2** (b), **PTPOP-3** (c), and **PTPOP-4** (d).

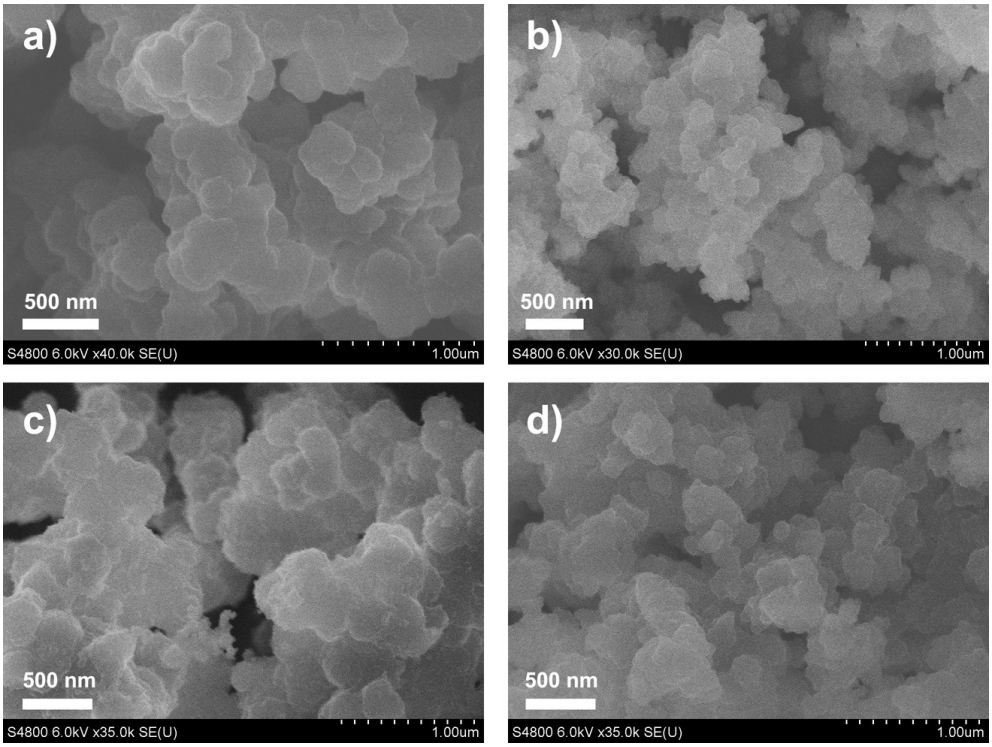

Fig. S4 FE-SEM images of **MTPOP-1** (a), **MTPOP-2** (b), **MTPOP-3** (c), and **MTPOP-4** (d).

Section D. HR-TEM images

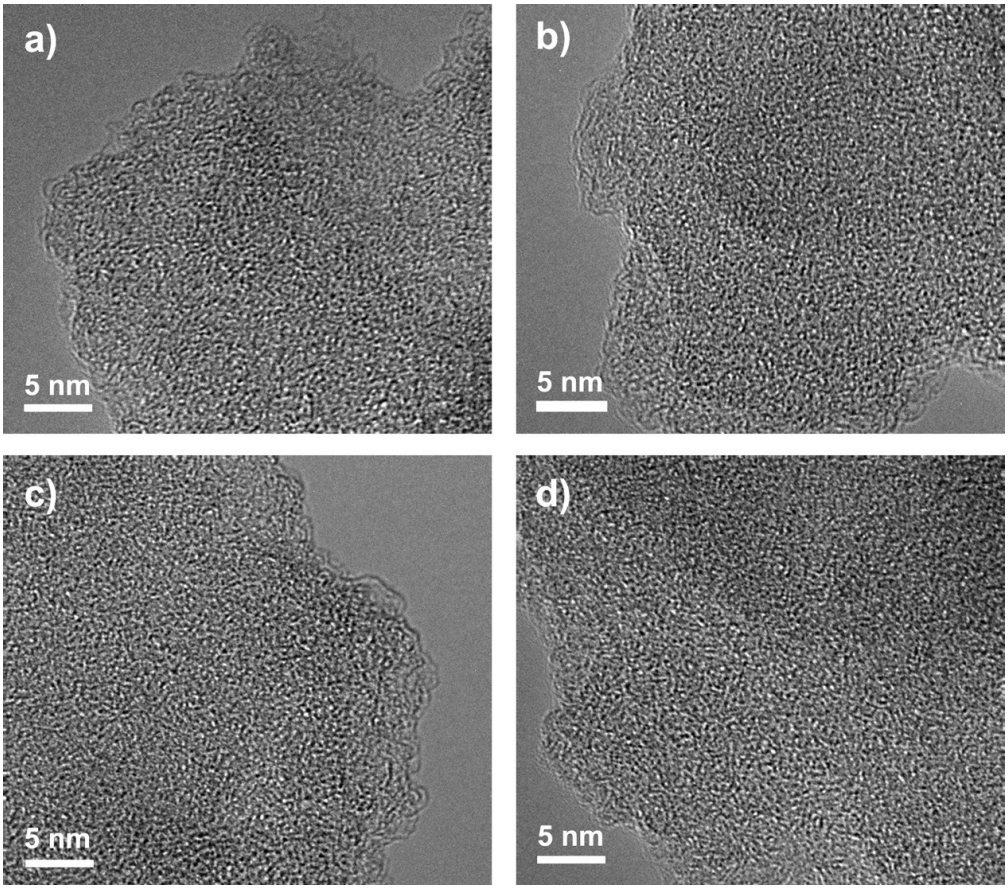

Fig. S5 HR-TEM images of **PTPOP-1** (a), **PTPOP-2** (b), **PTPOP-3** (c), and **PTPOP-4** (d).

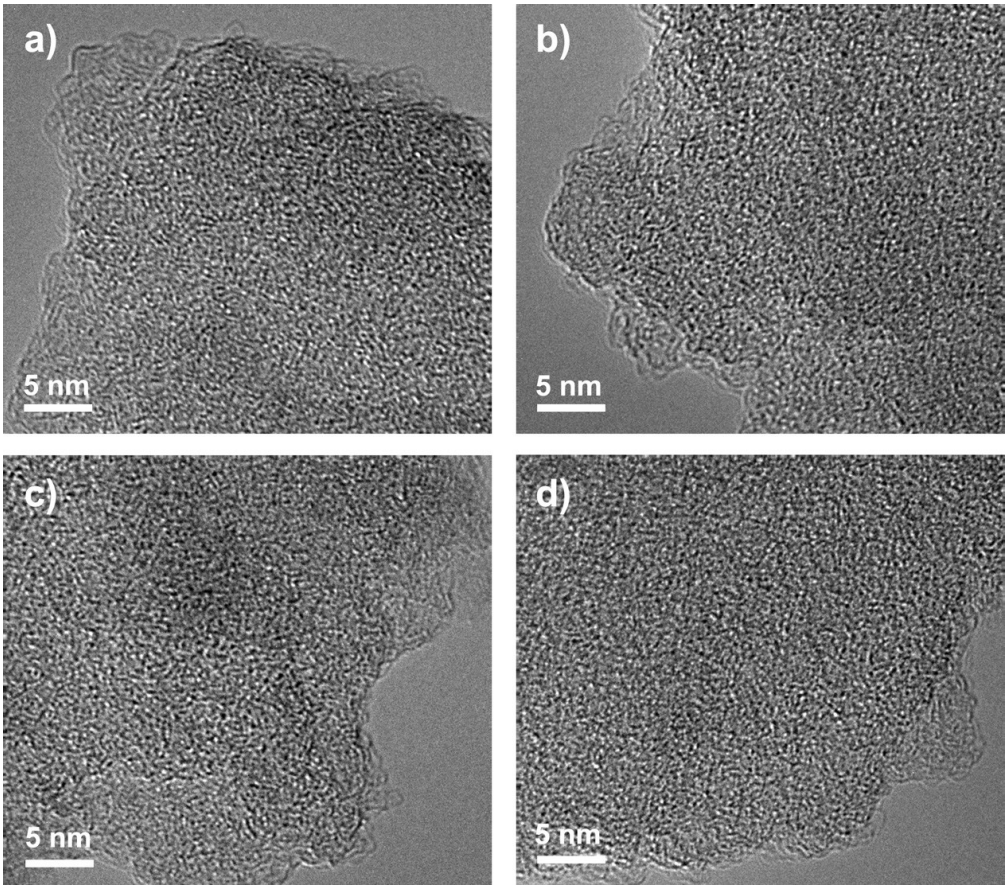

Fig. S6 HR-TEM images of **MTPOP-1** (a), **MTPOP-2** (b), **MTPOP-3** (c), and **MTPOP-4** (d).

Section E. FT-IR spectral profiles

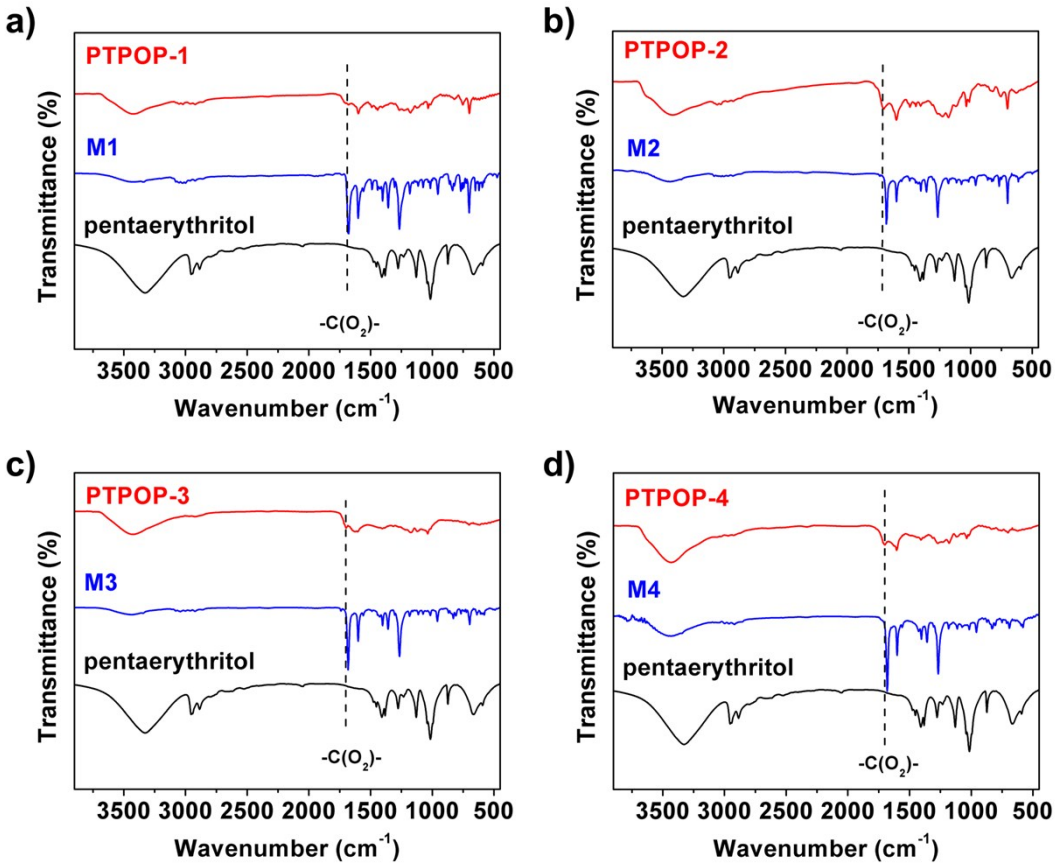

Fig. S7 FT-IR spectra of **PTPOP-1** (a), **PTPOP-2** (b), **PTPOP-3** (c), and **PTPOP-4** (d) compared with their monomers.

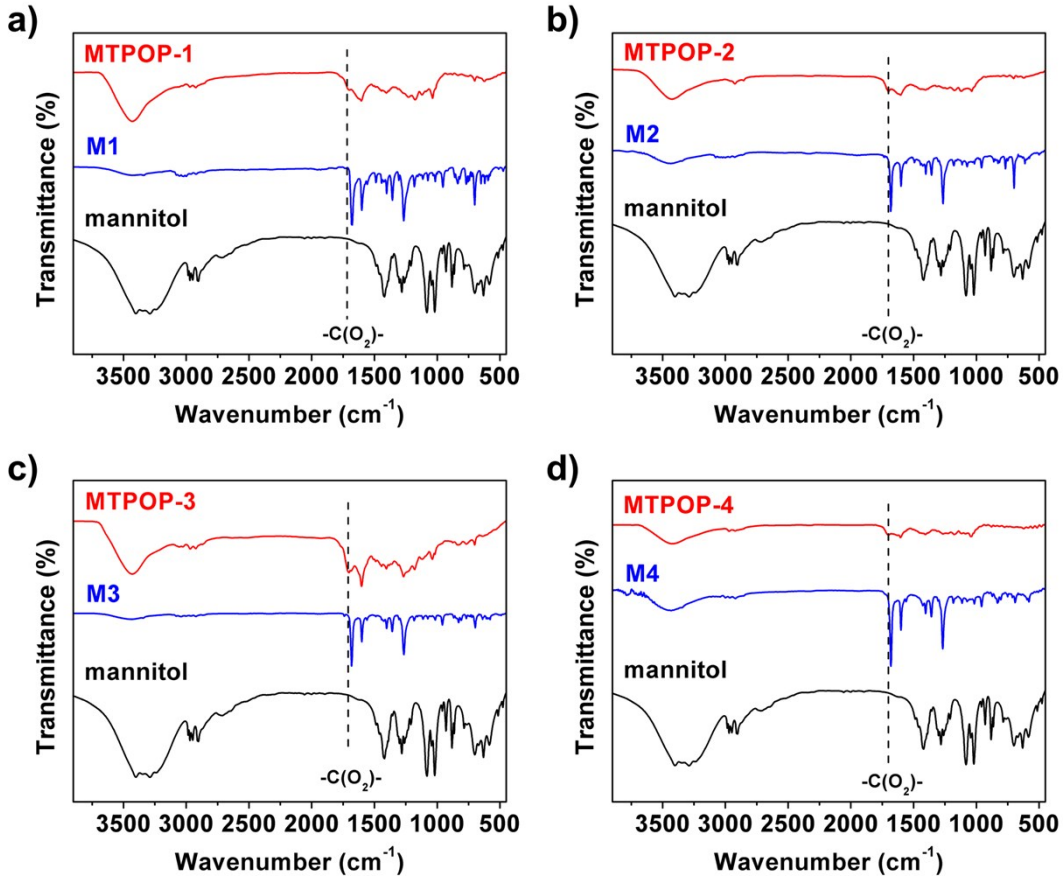

Fig. S8 FT-IR spectra of **MTPOP-1** (a), **MTPOP-2** (b), **MTPOP-3** (c), and **MTPOP-4** (d) compared with their monomers.

Section F. Solid-state ^{13}C CP/MAS NMR

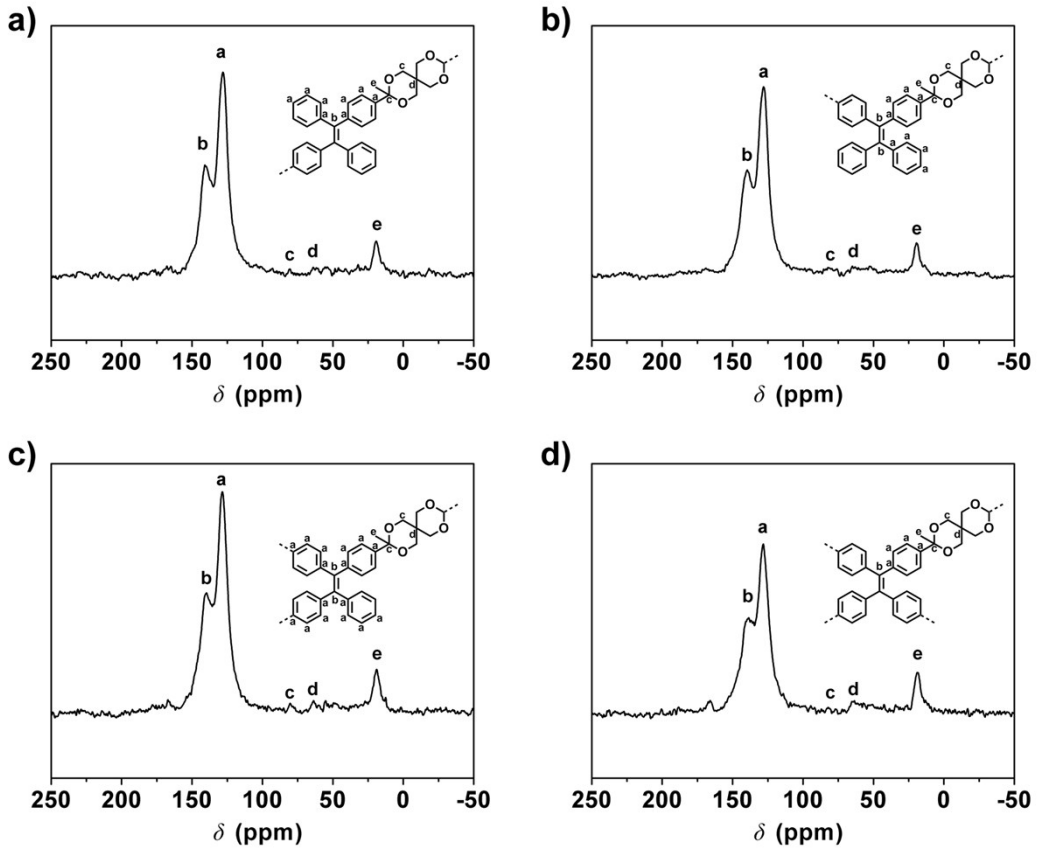

Fig. S9 Solid-state ^{13}C CP/MAS NMR spectrum of **PTPOP-1** (a), **PTPOP-2** (b), **PTPOP-3** (c), and **PTPOP-4** (d).

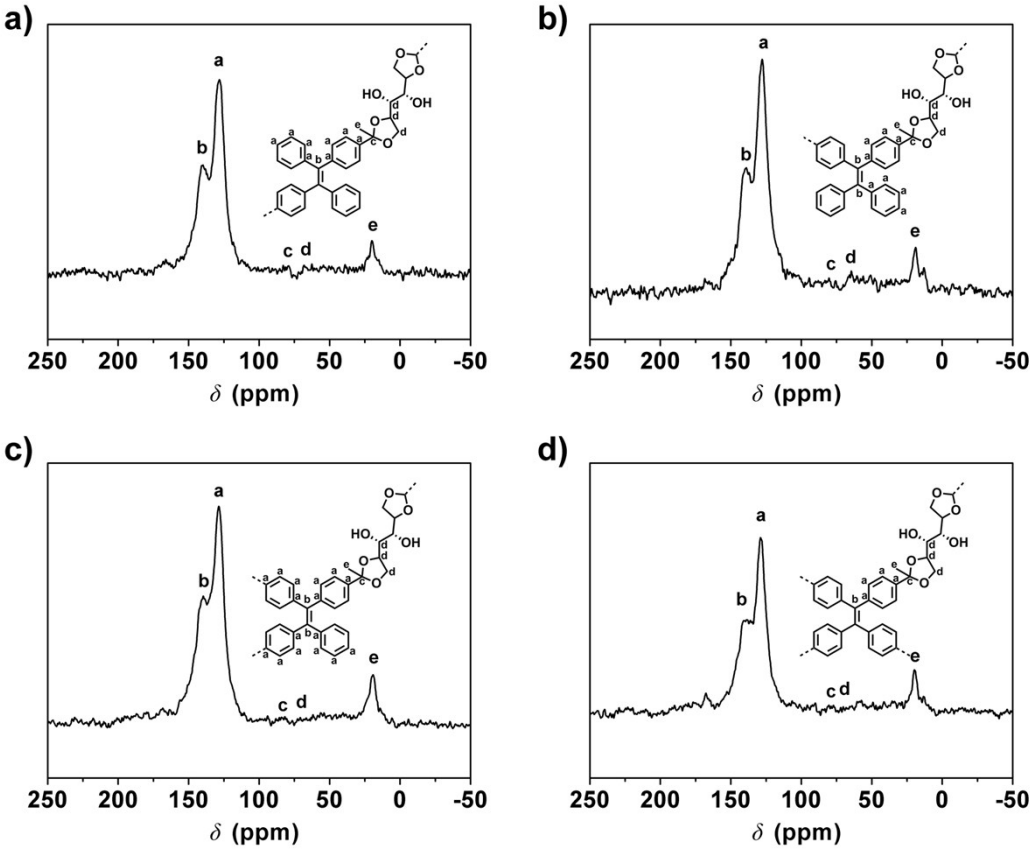

Fig. S10 Solid-state ^{13}C CP/MAS NMR spectrum of **MTPOP-1** (a), **MTPOP-2** (b), **MTPOP-3** (c), and **MTPOP-4** (d).

Section G. Corresponding data of porosity properties

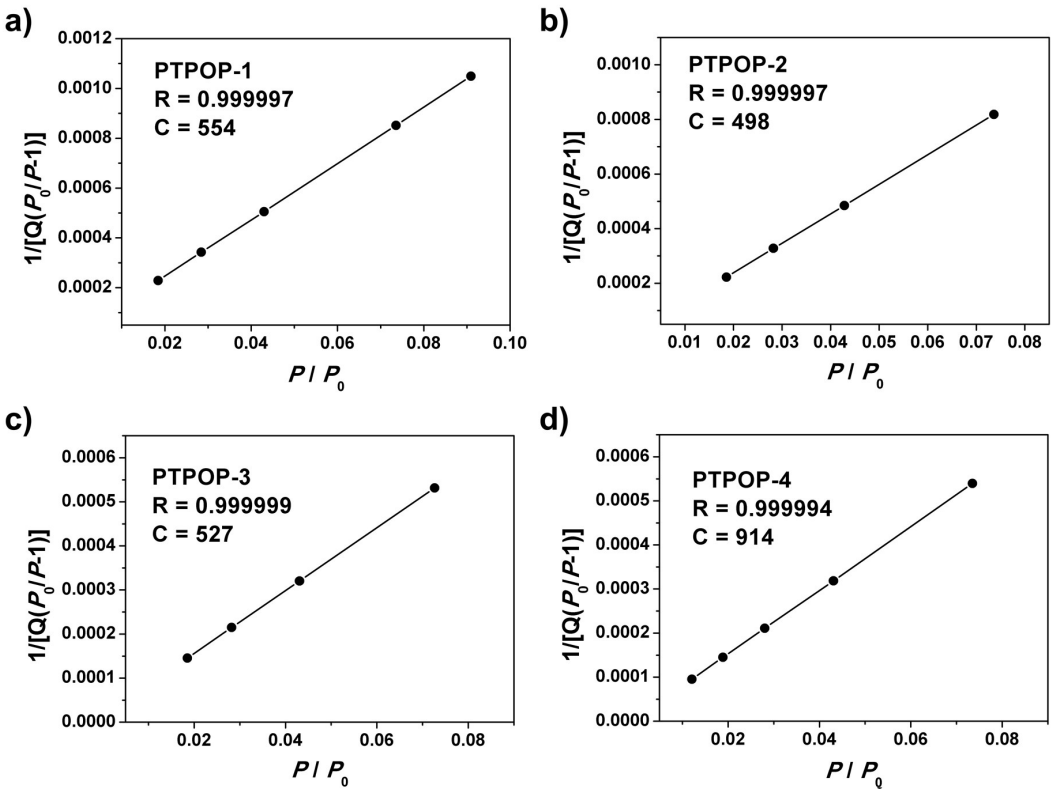

Fig. S11 BET plots of **PTPOP-1** (a), **PTPOP-2** (b), **PTPOP-3** (c), and **PTPOP-4** (d) from nitrogen adsorption data.

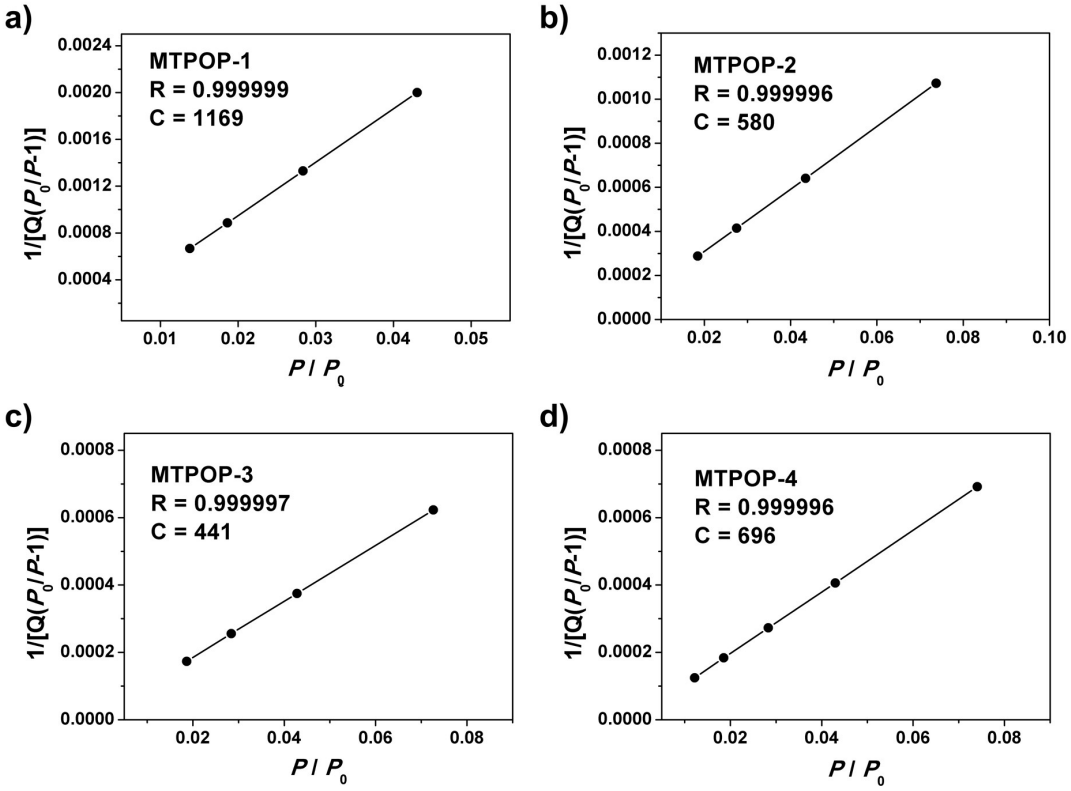

Fig. S12 BET plots of **MTPOP-1** (a), **MTPOP-2** (b), **MTPOP-3** (c), and **MTPOP-4** (d) from nitrogen adsorption data.

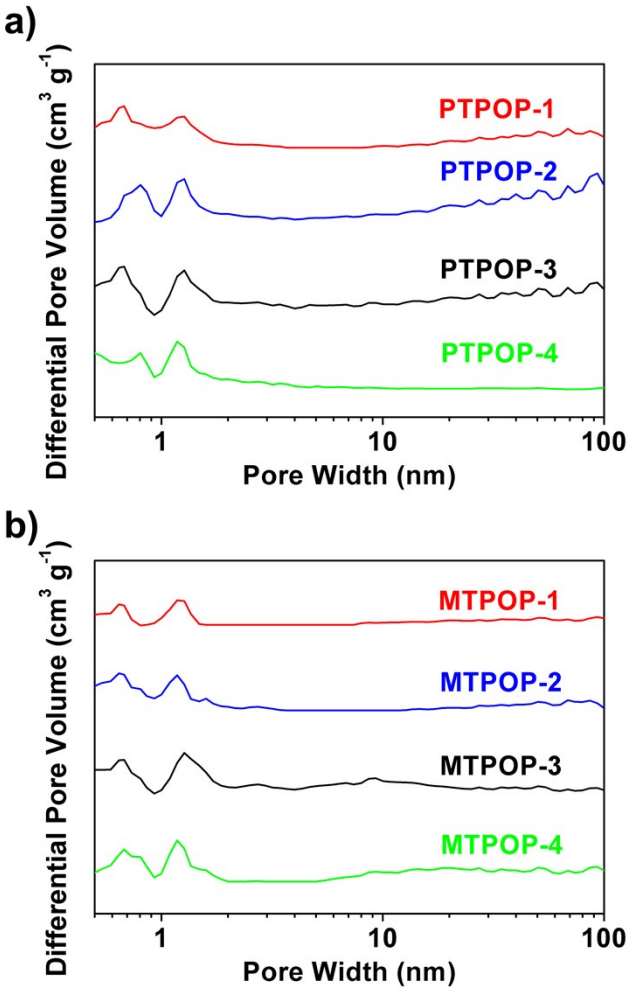

Fig. S13 Pore size distribution profiles calculated using the NLDFT method of **PTPOP-1–4** (a) and **MTPOP-1–4** (b).

Section H. Corresponding data of isosteric heats of adsorption

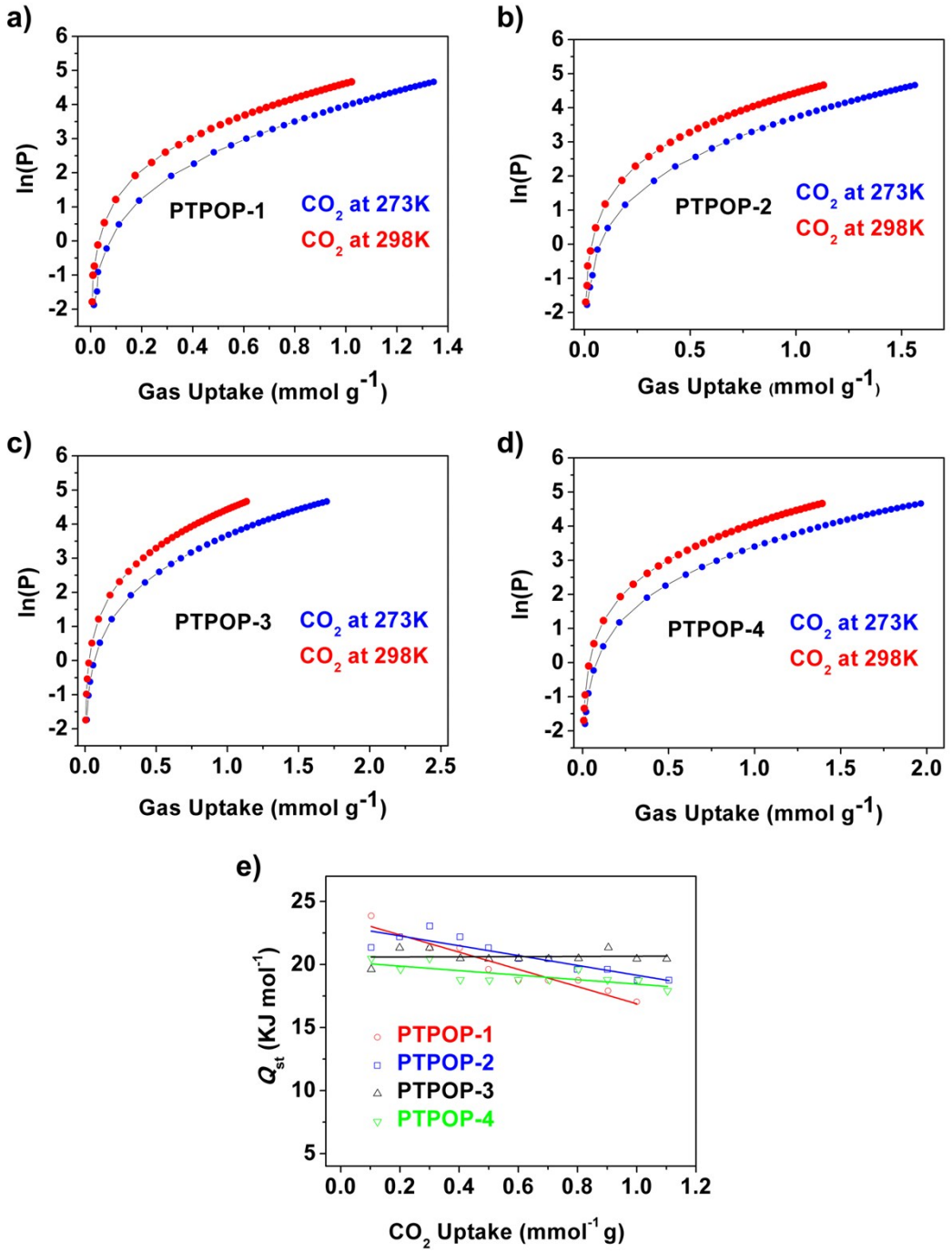

Fig. S14 Nonlinear curve fitting for **PTPOP-1** (a), **PTPOP-2** (b), **PTPOP-3** (c), and **PTPOP-4** (d) at different temperatures (273 and 298 K). (e) The isosteric heats of adsorption of CO_2 for **PTPOP-1–4**.

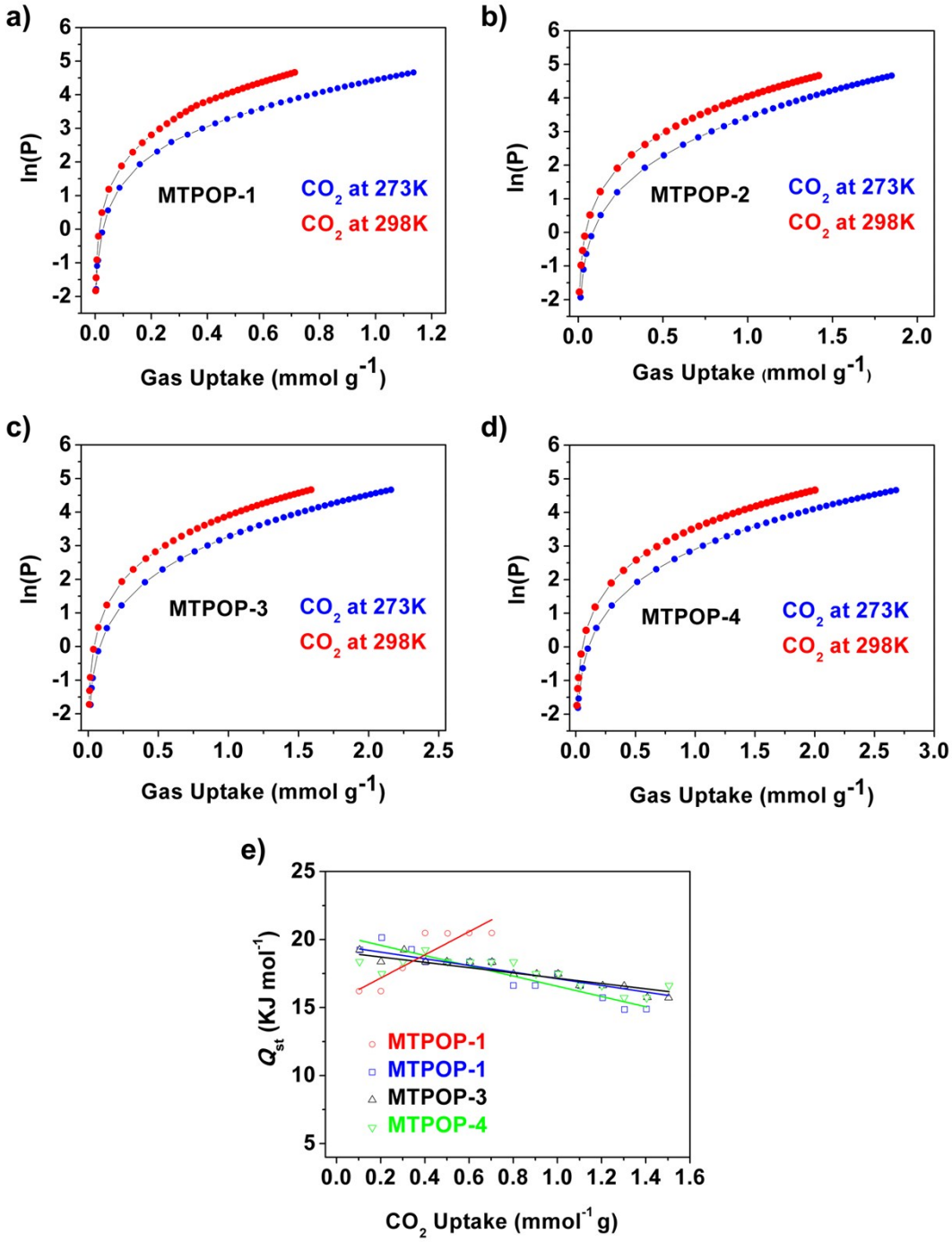

Fig. S15 Nonlinear curve fitting for **MTPOP-1** (a), **MTPOP-2** (b), **MTPOP-3** (c), and **MTPOP-4** (d) at different temperatures (273 and 298 K). (e) The isosteric heats of adsorption of CO_2 for **MTPOP-1–4**.

Section I. Corresponding data of gas selectivity analyses

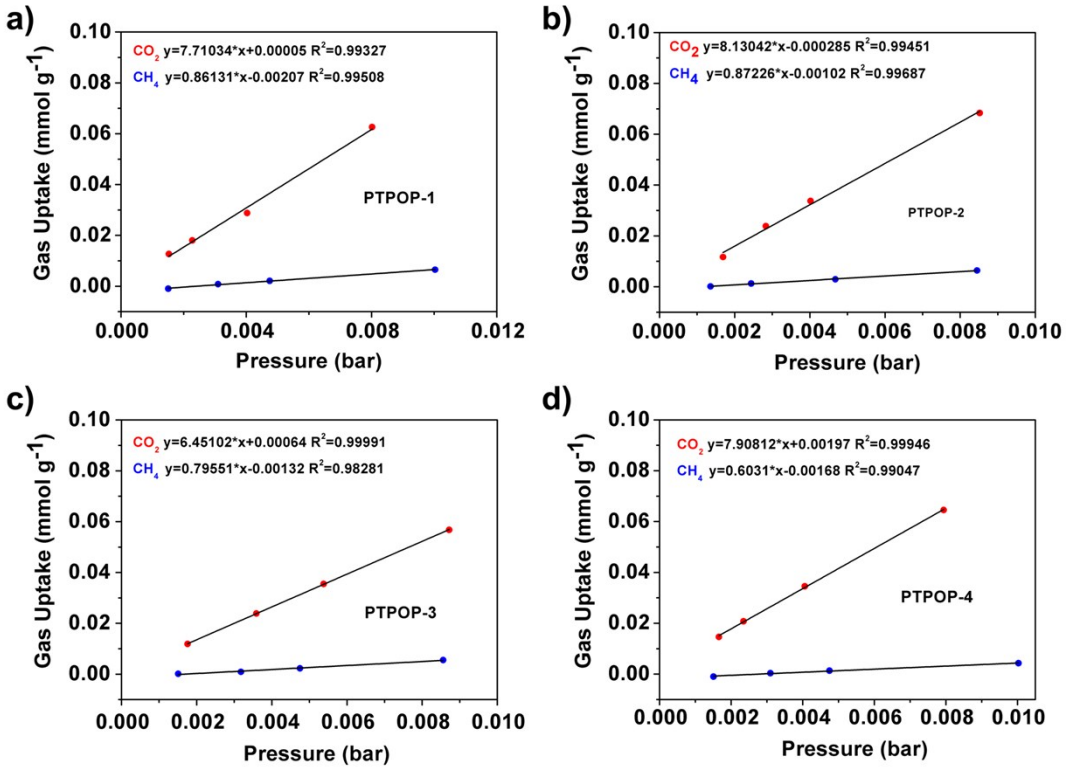

Fig. S16 CO_2/CH_4 initial slope selectivity studies for **PTPOP-1** (a), **PTPOP-2** (b), **PTPOP-3** (c), and **PTPOP-4** (d) at 273 K.

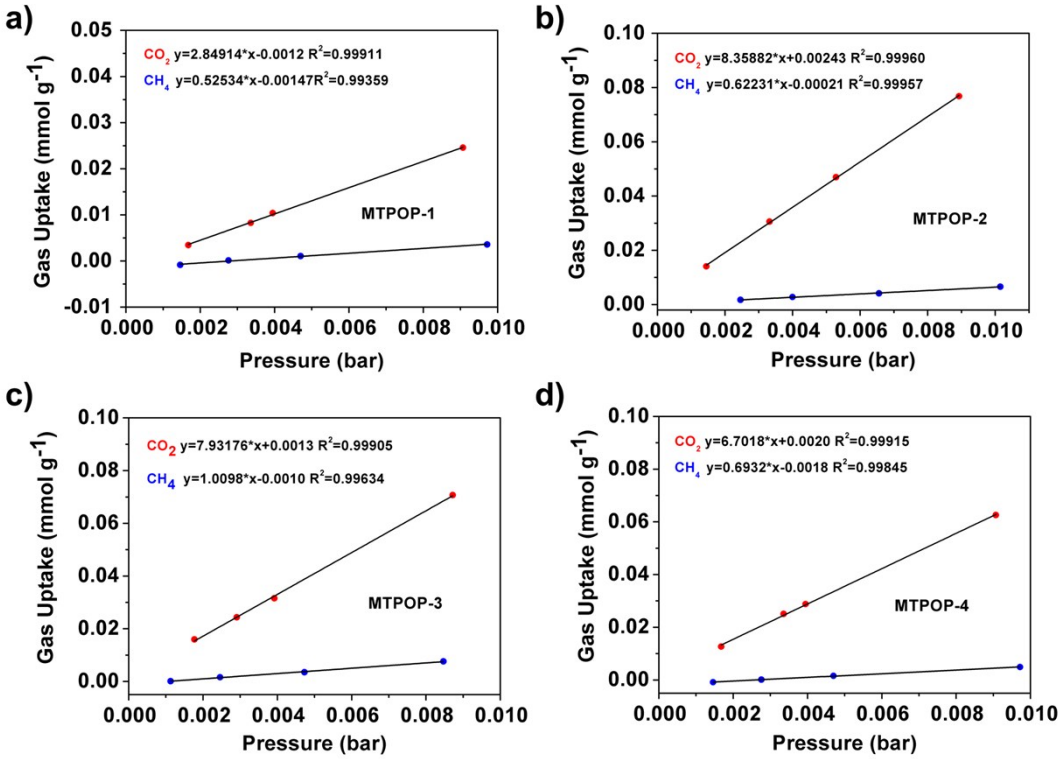

Fig. S17 CO_2/CH_4 initial slope selectivity studies for **MTPOP-1** (a), **MTPOP-2** (b), **MTPOP-3** (c), and **MTPOP-4** (d) at 273 K.

Ideal adsorbed solution theory (IAST) selectivity studies:

In order to evaluate the efficiency of **PTPOP-1–4** and **MTPOP-1–4** for CO_2 over CH_4 separation, we used the Ideal Adsorbed Solution Theory (IAST) of Myers and Prausnitz along with the pure component isotherm fits to determine the molar loadings in the mixture for specified partial pressures in the bulk gas phase.

The pure component isotherms of CO_2 measured at 273 K were fitted with the dual-site Langmuir (DSL) model:

$$q = q_A + q_B = q_{sat,A} \frac{b_A p}{1 + b_A p} + q_{sat,B} \frac{b_B p}{1 + b_B p}$$

The pure component isotherms of CH_4 measured at 273 K were fitted with the single-site Langmuir (SSL) model:

$$q = q_{sat,A} \frac{b_A p}{1 + b_A p}$$

where, q is molar loading of adsorbate (mmol g^{-1}), q_{sat} is saturation loading (mmol g^{-1}) , b is parameter in the pure component Langmuir isotherm (bar^{-1}), p is bulk gas phase pressure (bar).

Pure-component isotherm fitting parameters were then used for calculating IAST binary-gas adsorption selectivities (S_{ads}). S_{ads} is defined as:

$$S_{ads} = \frac{q_1/q_2}{p_1/p_2}$$

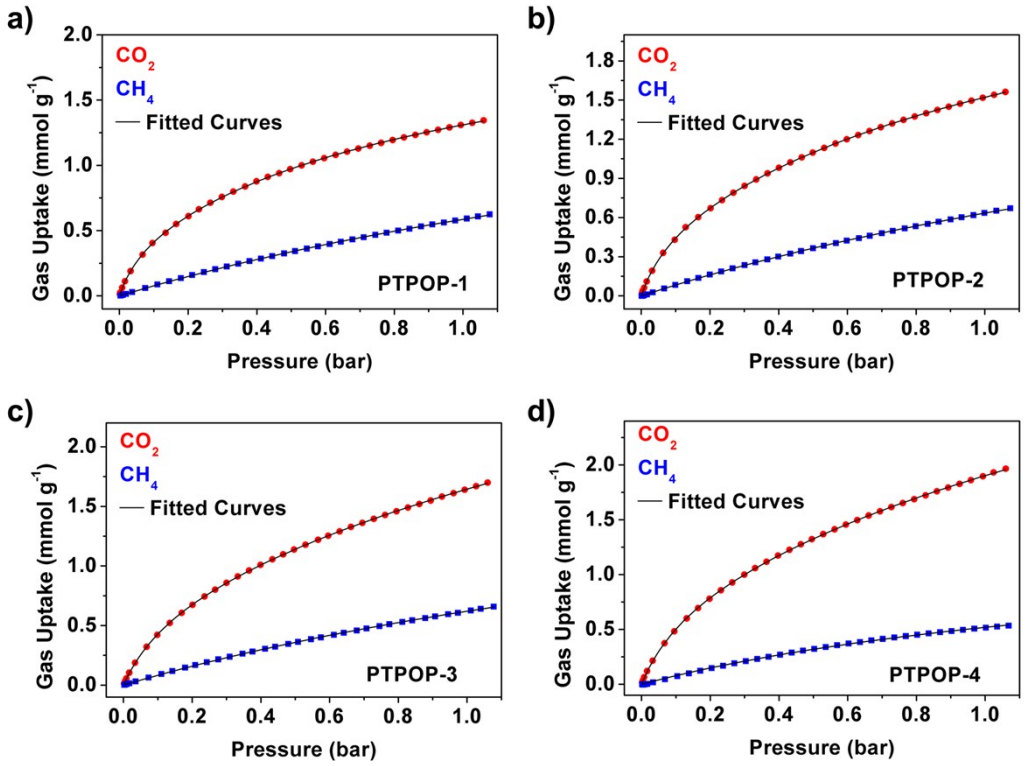

Fig. S18 The corresponding isotherm fits (solid black lines) dual-site Langmuir model fits for CO_2 and single-site Langmuir model for CH_4 of **PTPOP-1** (a), **PTPOP-2** (b), **PTPOP-3** (c), and **PTPOP-4** (d) based on experimental pure component isotherms for CO_2 (red circle) and CH_4 (blue circle) at 273 K.

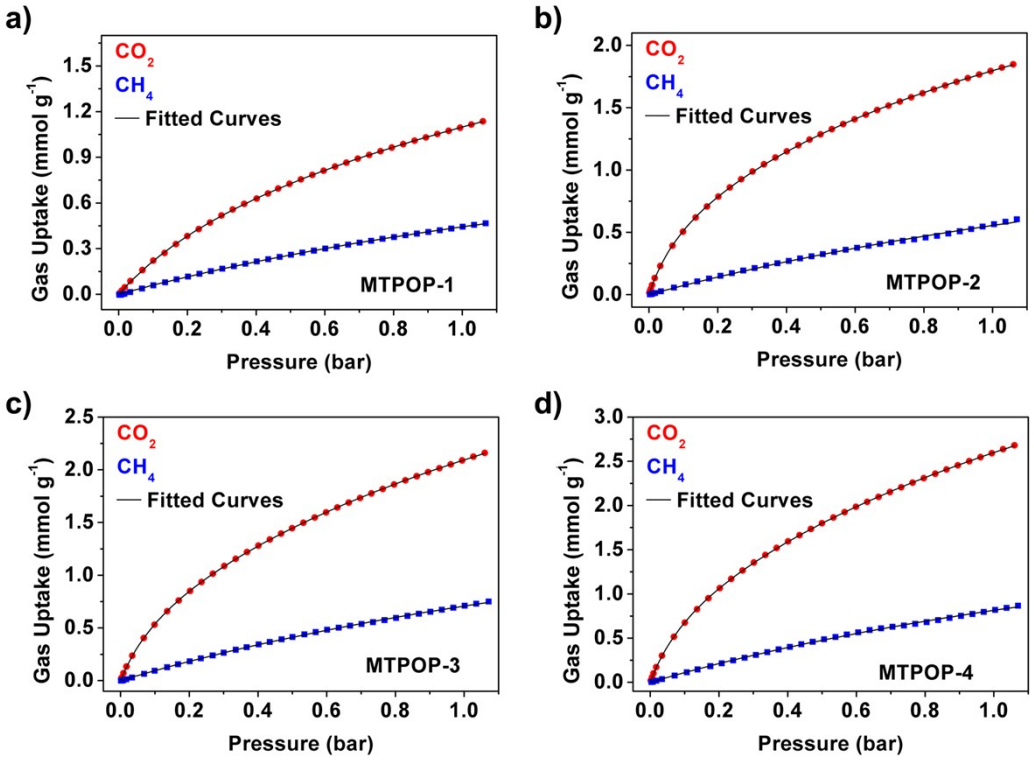

Fig. S19 The corresponding isotherm fits (solid black lines) dual-site Langmuir model fits for CO_2 and single-site Langmuir model for CH_4 of **MTPOP-1** (a), **MTPOP-2** (b), **MTPOP-3** (c), and **MTPOP-4** (d) based on experimental pure component isotherms for CO_2 (red circle) and CH_4 (blue circle) at 273 K.

Table S1 Langmuir fitting parameters of CO_2 and CH_4 adsorption isotherms of **PTPOP-1–4** and **MTPOP-1–4** at 273 K.

Polymers	Gas	$q_{sat,A}$ (mmol g^{-1})	b_A (bar^{-1})	$q_{sat,B}$ (mmol g^{-1})	b_B (bar^{-1})
PTPOP-1	CO_2	1.902	0.794	0.512	10.788
	CH_4	2.246	0.354		
PTPOP-2	CO_2	2.549	0.706	0.506	11.796
	CH_4	2.415	0.356		
PTPOP-3	CO_2	3.983	0.347	0.703	7.217
	CH_4	2.267	0.376		
PTPOP-4	CO_2	4.366	0.374	0.811	7.402
	CH_4	1.399	0.589		
MTPOP-1	CO_2	4.639	0.113	0.908	2.226
	CH_4	1.551	0.400		
MTPOP-2	CO_2	3.244	0.576	0.674	9.936
	CH_4	2.107	0.358		
MTPOP-3	CO_2	4.704	0.425	0.777	7.996
	CH_4	2.528	0.388		
MTPOP-4	CO_2	5.869	0.417	0.975	8.232
	CH_4	2.832	0.403		